Neurochemistry International 125 (2019) 175–186

Contents lists available at ScienceDirect

Neurochemistry International

journal homepage: www.elsevier.com/locate/neuint

Novel compound VB-037 inhibits Aβ aggregation and promotes neurite outgrowth through enhancement of HSP27 and reduction of P38 and JNK-mediated inflammation in cell models for Alzheimer's disease

Ya-Jen Chiu[a], Yu-Hsuan Hsieh[a], Te-Hsien Lin[a], Guan-Chiun Lee[a], Hsiu Mei Hsieh-Li[a], Ying-Chieh Sun[b], Chiung-Mei Chen[c], Kuo-Hsuan Chang[c,*], Guey-Jen Lee-Chen[a,**]

[a] Department of Life Science, National Taiwan Normal University, Taipei, 11677, Taiwan
[b] Department of Chemistry, National Taiwan Normal University, Taipei, 11677, Taiwan
[c] Department of Neurology, Chang Gung Memorial Hospital, Chang Gung University College of Medicine, Taoyuan, 33302, Taiwan

ARTICLE INFO

Keywords:
Alzheimer's disease
Aβ aggregation
Synthetic quinoline derivatives
P38/JNK signaling pathways
Therapeutics

ABSTRACT

The pathogenesis of Alzheimer's disease (AD) is involved in the aggregation of misfolded amyloid β (Aβ), which upregulates the activity of acetylcholinesterase (AChE), increases the production of reactive oxygen species (ROS), enhances neuroinflammation, and eventually leads to neuronal death. Therefore, compounds targeting these mechanisms may be candidates for multitarget drugs in AD treatment. We found that two quinoline derivatives, VB-030 and VB-037, markedly reduced Aβ aggregation and ROS levels in the thioflavin T biochemical assay and Tet-On Aβ-green fluorescent protein (GFP) 293 AD cell model. These compounds further improved neurite outgrowth, reduced AChE activity and upregulated the molecular chaperone heat shock protein family B [small] member 1 (HSP27), whereas knockdown of HSP27 counteracted the compounds' neuroprotective effects on the Tet-On Aβ-GFP SH-SY5Y AD neuronal model. Furthermore, VB-037 attenuated lipopolysaccharide (LPS)/interferon (IFN)-γ-induced activation of BV-2 microglial cells. In addition, VB-037 demonstrated its potential to diminish LPS/IFN-γ-induced upregulation of caspase 1 activity, expression of interleukin (IL)-1β, and active phosphorylation of mitogen-activated protein kinase 14 (P38), mitogen-activated protein kinase 8 (JNK), and Jun proto-oncogene, AP-1 transcription factor subunit (JUN) signalings, as well as improve cell viability in the Tet-On Aβ-GFP SH-SY5Y AD neuronal model. Our findings strongly indicate the potential of VB-037 for modifying AD progression by targeting multiple mechanisms, thereby offering a new drug development avenue for AD treatment.

1. Introduction

Alzheimer's disease (AD) is the most common form of dementia among older people (Querfurth and LaFerla, 2010). Past AD research suggested that accumulations of abnormally folded amyloid-β (Aβ) and tau proteins in amyloid plaques and neurofibrillary tangles are causally related to neurodegenerative processes in the brains of AD patients (Scheltens et al., 2016). Studies of familial AD patients with mutations in the amyloid precursor protein (APP), presenilin 1 (PSEN1), or presenilin 2 (PSEN2) (Hardy, 1997) have provided strong evidence for Aβ being the trigger or driver of the disease process (Selkoe and Hardy, 2016). APP is the precursor of the Aβ (da Cruz e Silva and da Cruz e Silva, 2003) and APP mutations affect Aβ cleavage and aggregation (Scheltens et al., 2016). PSEN1 and PSEN2 provide the catalytic subunit to the γ-secretases, which cleave APP (Takasugi et al., 2003). Aβ spontaneously aggregates into oligomers and coalesces to form insoluble fibrils, which attract and activate microglia (Sondag et al., 2009), resulting in production of proinflammatory cytokines, including interleukin (IL)-1β, IL-6, tumor necrosis factor (TNF)-α and interferon (IFN)-γ (Wang et al., 2015a). These cytokines potentiate production and dispersal of Aβ oligomers (Dal Prà et al., 2015). Furthermore, exposure of neurons to Aβ oligomers upregulates the level of Toll-like receptor (TLR)-4 (Calvo-Rodríguez et al., 2017), which mediated memory impairment in an acute mouse model of AD (Balducci et al., 2017). Therefore, strategies to minimize the production of Aβ while inhibiting neuroinflammation are the mainstream of AD therapy development.

Quinoline is a heterocyclic aromatic organic compound with the chemical formula C_9H_7N. Quinoline derivatives have received

* Corresponding author. Chang Gung Memorial Hospital, Chang Gung University College of Medicine, Taoyuan 33302, Taiwan.
** Corresponding author. National Taiwan Normal University, Taipei 11677, Taiwan.
E-mail addresses: gophy5128@cgmh.org.tw (K.-H. Chang), t43019@ntnu.edu.tw (G.-J. Lee-Chen).

https://doi.org/10.1016/j.neuint.2019.01.021
Received 10 September 2018; Received in revised form 21 January 2019; Accepted 25 January 2019
Available online 29 January 2019
0197-0186/

considerable attention because they exhibit various antimicrobial activities (Abdallah et al., 2006; Eswaran et al., 2010; Desai et al., 2013; Pitta et al., 2016). Several quinolines have exerted inhibitory effects on the aggregation of amyloidogenic proteins such as lysozyme (Lieu et al., 2007), tau (Pickhardt et al., 2005; Navarrete et al., 2012; Chang et al., 2017), and Aβ (Wang et al., 2015b; Chang et al., 2016; Jones et al., 2016). In addition, the quinoline framework has emerged as a new template for the design and identification of novel anti-inflammatory agents (Mukherjee and Pal, 2013). Cryptolepine—an quinoline derivative found in *Cryptolepis sanguinolenta*—inhibits lipopolysaccharide (LPS)-induced microglial activation and production of TNF-α, IL-6, IL-1β, nitric oxide (NO), and prostaglandin E2 (PGE2) (Olajide et al., 2013). Moreover, a reported cyclopentaquinoline hybrid that demonstrates acetylcholinesterase (AChE) and Aβ aggregation inhibitory activities and has anti-inflammatory properties can be a new multi-targeted treatment option for AD (Czarnecka et al., 2017). In the present study, we examined the potential of two quinoline compounds (VB-030 and VB-037) for modulating Aβ-mediated toxicity. In addition, we evaluated whether VB-037 can inhibit microglial activation and neuroinflammation.

2. Materials and methods

2.1. Compounds and cell culture

Curcumin was purchased from Sigma-Aldrich (St. Louis, MO, USA). VB-030 (product ID: Z1157726443) and VB-037 (product ID: Z46595412) were purchased from Enamine (Kiev, Ukraine). All three compounds were soluble in a cell culture medium up to 100 μM.

Human Aβ-green fluorescent protein (GFP) 293 and SH-SY5Y cells (Chang et al., 2016) were maintained in Dulbecco's modified Eagle's medium (DMEM) (for 293 cells) or DMEM-F12 (for SH-SY5Y cells) supplemented with 10% fetal bovine serum (FBS) (Thermo Fisher Scientific, Waltham, MA, USA), with 5 μg/mL blasticidin and 100 μg/mL hygromycin (InvivoGen, San Diego, CA, USA) added to the growth medium. Mouse BV-2 microglial cells were derived from primary mouse microglial cells (Blasi et al., 1990) (provided by Dr. Han-Min Chen, Catholic Fu-Jen University, New Taipei City, Taiwan) and cultivated in DMEM containing 10% FBS.

2.2. Thioflavin T binding assay

To stain amyloid, the $A\beta_{42}$ peptide (final concentration: 5 μM; AnaSpec, Fremont, CA, USA) was incubated with curcumin (as a positive control) (Yang et al., 2005), VB-030, or VB-037 (5–20 μM) in 150 mM NaCl and 20 mM Tris-HCl (pH8.0) at 37 °C for 48 h (LeVine, 1999). To measure Aβ aggregation, thioflavin T (final concentration: 10 μM; Sigma-Aldrich) was added and incubated for 5 min at room temperature and the fluorescence intensity of samples was recorded at excitation/emission wavelengths of 420/485 nm by using the FLx800 microplate reader (Bio-Tek, Winooski, VT, USA).

2.3. BV-2 cell cytotoxicity assay

BV-2 cells were seeded on a 48-well plate (5×10^3/well) and treated with VB-030 or VB-037 (1–100 μM) for 24 h. Cell viability was measured based on reduction of 3, (4,5-dimethylthiazol-2-yl)-2,5-diphenyltetrazolium bromide (MTT). Absorbance of the insoluble purple formazan dye was measured at 570 nm on the μQuant microplate spectrophotometer (Bio-Tek). Half-maximal inhibitory concentration (IC_{50}) was defined as the concentration of compounds required for reduction of 570-nm signals by 50%.

2.4. Aβ-GFP 293 cell fluorescence and cytotoxicity assays

On day 1, cells were seeded on a 96-well plate (8×10^3/well). On day 2, the cells were pretreated with curcumin, VB-030, or VB-037 (1.2–10 μM) for 8 h followed by induction of Aβ-GFP expression with doxycycline (2 μg/mL; Sigma-Aldrich). On day 5, the cells were stained with Hoechst 33342 (0.1 μg/mL; Sigma-Aldrich) for 30 min; cell images were automatically recorded at excitation/emission wavelengths of 482/436 nm by using the ImageXpress Micro Confocal High-Content Imaging System (Molecular Devices, Sunnyvale, CA, USA) and analyzed using MetaXpress Image Acquisition and Analysis Software (Molecular Devices). Relative GFP fluorescence was measured only if the proportion of survived cells was greater than 80% of that of nontreated cells. In addition, cell number counted by nucleus staining was used to measure the cytotoxicity of test compounds in 293 cells expressing Aβ-GFP.

2.5. Aβ-GFP RNA analysis

On day 1, cells were seeded on a 6-well plate (3×10^5/well). Curcumin, VB-030, or VB-037 (5 μM) treatment and Aβ-GFP induction were performed on day 2 as described. To measure Aβ-GFP RNA on day 5, total RNA was extracted using TRIzol reagent, treated with DNase to remove chromosomal DNA, and used for cDNA synthesis with SuperScript™ III reverse transcriptase (Thermo Fisher Scientific). Relative Aβ-GFP expression was analyzed in 100 ng cDNA through quantitative, real-time and fluorogenic polymerase chain reaction (PCR) (StepOnePlus™ Real-time PCR system; Applied Biosystems, Foster City, CA, USA) with TaqMan probes PN4331348 for enhanced GFP and 4326321E for hypoxanthine phosphoribosyltransferase 1 (HPRT1) control (Applied Biosystems).

2.6. Reactive oxygen species analysis

Aβ-GFP 293 cells were seeded on a 12-well plate (6×10^4/well) and treated with a tested compound (5 μM); then, Aβ-GFP expression was induced as described. On day 5, CellROX™ Deep Red (Molecular Probes, Waltham, MA, USA) was added to a final concentration of 5 μM and incubated at 37 °C for 30 min. Reactive oxygen species (ROS) in cells was measured using a flow cytometer (Becton Dickinson, Franklin Lakes, NJ, USA) with excitation/emission wavelengths of 633/661 ± 8 nm (FL4 channel).

2.7. Neurite outgrowth analysis

On day 1, Aβ-GFP SH-SY5Y cells were seeded on a 24-well plate (3×10^4/well) with retinoic acid (10 μM; Sigma-Aldrich) added to induce neuronal differentiation (Pahlman et al., 1984). On day 2, the cells were treated with a test compound (5 μM) and Aβ-GFP expression was induced as described. On day 8, after being fixed (4% paraformaldehyde for 15 min), permeabilized (0.1% Triton X-100 for 10 min), and blocked (3% bovine serum albumin for 20 min), the cells were stained with primary neuronal class III β-tubulin (TUBB3) antibody (1:1000, #MMS-435P) (Covance, Princeton, NJ, USA) at 4 °C overnight, followed by a secondary donkey antirabbit Alexa Fluor ®555 antibody (1:1000, #A-31572) (Thermo Fisher Scientific) at room temperature for 3 h. After nuclei were stained with 4',6-diamidino-2-phenylindole (DAPI; 0.1 μg/mL; Sigma-Aldrich) for 30 min, neuronal images were captured using a high-content analysis (HCA) system as described and analyzed using the Neurite Outgrowth Application Module (Molecular Devices).

2.8. AChE assay

As described, Aβ-GFP SH-SY5Y cells were seeded on a 6-well plate (4×10^5/well) with retinoic acid (added on day 1) and treated with a test compound (5 μM); induction of Aβ-GFP expression followed on day 2. On day 8, the cells were collected, resuspended in cold phosphate-buffered saline, and lysed through sonication. After centrifugation to collect the supernatant, AChE activity was measured using the AChE

activity assay kit (Sigma-Aldrich) with 20 μg cell extracts. The mixture was incubated for 2–10 min at room temperature and absorbance at 412 nm was measured using the Multiskan™ GO spectrophotometer (Thermo Fisher Scientific).

2.9. Propidium iodide cell cytotoxicity assay

As described, Aβ-GFP SH-SY5Y cells were seeded on a 12-well plate (1×10^5/well) with retinoic acid (added on day 1) and treated with a test compound (1.2–10 μM); induction of Aβ-GFP expression followed on day 2. On day 8, cell viability was evaluated through propidium iodide (PI; 12 μg/mL; Sigma-Aldrich) staining (37 °C for 30 min) and flow cytometric quantitation (excitation and emission wavelengths of 488 and 585 ± 21 nm, respectively) (FL2 channel, Becton-Dickinson). In addition, after removal of retinoic acid, differentiated Aβ-GFP SH-SY5Y cells were stimulated with LPS (1 μg/mL; Sigma-Aldrich) and IFN-γ (0.1 μg/mL; PeproTech, Rocky Hill, NJ, USA) on day 6, and cell viability was assessed through PI staining and flow cytometry on day 8.

2.10. NO and induction of brown adipocytes 1 assays

On day 1, BV-2 cells were seeded on a 12-well plate (1×10^5/well) in a medium containing 1% FBS. On day 2, the cells were pretreated with VB-037 (10 μM) for 8 h, followed by LPS (1 μg/mL) and IFN-γ (0.1 μg/mL) treatment for 20 h to induce activation. On day 3, the NO level in the cultured medium was measured using the Griess reagent kit (Thermo Fisher Scientific). Induction of brown adipocytes 1 (Iba1) level in activated BV-2 cells was examined through Western blotting (1:500 anti-Iba1 antibody, Wako, Osaka, Japan).

2.11. Caspase 1 activity and IL-1β/TNF-α/IL-6 enzyme-linked immunosorbent assays

As described, Aβ-GFP SH-SY5Y cells were seeded on a 12-well plate (1×10^5/well) with retinoic acid (added on day 1) and treated with a test compound (5 μM); induction of Aβ-GFP expression followed on day 2 and stimulation with LPS/IFN-γ was performed on day 6. On day 8, caspase 1 activity in cells was assessed using the IL-1β-converting enzyme (ICE) fluorimetric assay kit (BioVision, Milpitas, CA, USA), with excitation/emission wavelengths of 400/505 nm (FLx800 fluorescence microplate reader, Bio-Tek). In addition, IL-1β, TNF-α and IL-6 were measured using the enzyme-linked immunosorbent assay Ready-SET-Go reagent (eBioscience, San Diego, CA, USA). All experimental procedures were performed following the corresponding manufacturers' instructions.

2.12. RNA interference

To knockdown expression of heat shock protein family B [small] member 1 (HSP27) in Aβ-GFP SH-SY5Y cells, lentiviruses with short hairpin RNA (shRNA) targeting HSP27 (TRCN0000008753) and a negative control scrambled shRNA (TRC2.Void) were obtained from National RNAi Core Facility, Institute of Molecular Biology/Genomic Research Center, Academia Sinica, Taipei, Taiwan. On day 1, cells were plated on 6-well plates (6×10^5/well for protein analysis) or 24-well plates (2×10^4/well for neurite outgrowth analysis) in the presence of retinoic acid as described. On day 2, the cells were infected with lentivirus (multiplicity of infection: 3) in the presence of polybrene (8 μg/mL; Sigma-Aldrich) to increase infectivity. On day 3, the cells were pretreated with a compound (5 μM) for 8 h; induction of Aβ-GFP expression followed. On day 9, the cells were collected for HSP27 and Aβ-GFP protein analysis or analyzed for neurite outgrowth as described.

2.13. Western blot

Total proteins from Aβ-GFP SH-SY5Y cells were obtained using a lysis buffer containing 50 mM Tris-HCl (pH8.0), 150 mM NaCl, 1 mM ethylenediaminetetraacetic acid (pH8.0), 1 mM ethylene glycol tetraacetic acid (pH8.0), 0.1% sodium dodecyl sulfate (SDS), 0.5% sodium deoxycholate, 1% Triton X-100 and a protease inhibitor cocktail (Sigma-Aldrich). After quantitation using a protein assay kit (Bio-Rad, Hercules, CA, USA), proteins (20 μg) were separated on 10% SDS-polyacrylamide gel electrophoresis and blotted onto polyvinylidene difluoride membranes (Sigma-Aldrich) through reverse electrophoresis. After blocking, the membrane was probed with antibodies against HSP27 (1:500, #sc-1049), GFP (1:500, #sc-9996) (Santa Cruz Biotechnology, Santa Cruz, CA, USA), mitogen-activated protein kinase 14 (P38) (1:2000, #9212), phospho-P38 (T180/Y182) (1:1000, #9216), mitogen-activated protein kinase 8 (JNK) (1:1000, #9252), phospho-JNK (T183/Y185) (1:1000, #9255), Jun proto-oncogene, AP-1 transcription factor subunit (JUN) (1:2000, #9165), phospho-JUN (S63) (1:1000, #9261) (Cell Signaling Technology, Danvers, MA, USA), glyceraldehyde-3-phosphate dehydrogenase (GAPDH) (1:1000, #30000002) (MDBio Inc., Taipei, Taiwan), or β-actin (1:5000, #MABT825) (Millipore, Billerica, MA, USA). Subsequently, immune complexes were detected using a horseradish peroxidase-conjugated goat antimouse (1:5000, #GTX77315) or goat antirabbit (1:5000, #GTX77060) IgG antibody (GeneTex, Irvive, CA, USA) and a chemiluminescent substrate (Millipore).

2.14. Statistical analysis

Data are presented as the mean ± standard deviation of three independent experiments. Differences between groups were evaluated using a two-tailed Student's *t*-test or analysis of variance (one way and two way) with a *post hoc* LSD test where appropriate. A P value lower than 0.05 was considered statistically significant.

3. Results

3.1. Tested compounds and Aβ aggregation inhibition

Two compounds, namely VB-030 and VB-037 (Fig. 1A), were tested. In addition, curcumin—a potent Aβ aggregate inhibitor (Yang et al., 2005)—was included for comparison. The results of the thioflavin T assay, which was widely used to measure the misfolded level of amyloid (LeVine, 1999), indicated that curcumin, VB-030, and VB-037 all demonstrated significant aggregation inhibition, with half-maximal effective concentration (EC_{50}) of < 5, 30, and 8 μM, respectively (Fig. 1B). Furthermore, we evaluated the aggregation-inhibitory effects of tested compounds on the established Tet-On Aβ-GFP 293 cells (Fig. 1C). In the Aβ-GFP fusion protein, Aβ aggregated rapidly, resulting in misfolding of the fused GFP, which reduced the fluorescence intensity. Inhibition of Aβ aggregation may improve GFP folding, thereby increasing the fluorescent signal in Aβ-GFP-expressing cells (Zhao et al., 2012). Fig. 1D shows the representative fluorescent images of Aβ-GFP-expressing cells treated with or without curcumin or VB-037 (5 μM). As a positive control, the green fluorescence intensity of cells pretreated with 1.2–5 μM curcumin increased significantly (102%–120%, $P = 0.021$ to < 0.001) compared with untreated cells (100%). Treatment with VB-030 (116%–124%, $P < 0.001$) or VB-037 (127%–134%, $P < 0.001$) at 1.2–10 μM also significantly increased the green fluorescence intensity (Fig. 1E). In Aβ-GFP-expressing 293 cells, curcumin, VB-030, and VB-037 had IC_{50} values of 10, 22, and 76 μM, respectively. Treatment with curcumin, VB-030, and VB-037 (5 μM) did not significantly alter the Aβ-GFP RNA level (101%–105%, $P > 0.05$) compared with untreated cells (100%) (Fig. 1F), indicating that the increase in fluorescence intensity was not due to the change in gene expression. In the oxidative stress analysis, Aβ-GFP expression significantly elevated the ROS level of Aβ-GFP-expressing 293 cells (126%, $P < 0.001$), whereas treatment with curcumin, VB-030, or VB-037 (5 μM) effectively reduced the ROS level associated with Aβ

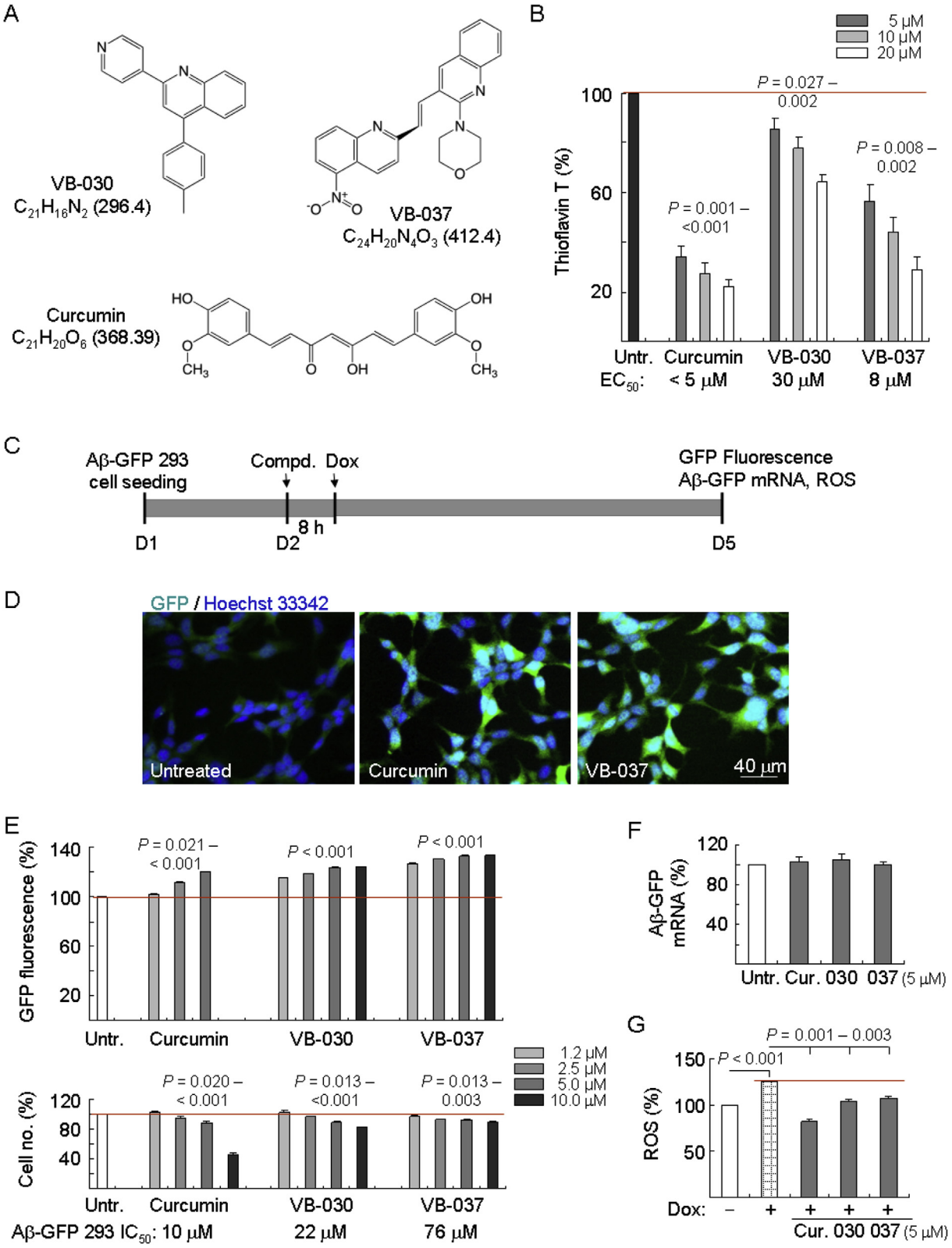

Fig. 1. Prevention of Aβ aggregation and antioxidation of test compounds. (A) Structure, formula and MW of VB-030, VB-037, and curcumin. (B) Aβ aggregation inhibition of curcumin, VB-030, and VB-037 (5–20 μM) by the thioflavin T assay ($n = 3$). To normalize, the relative thioflavin T fluorescence of $A\beta_{42}$ without compound treatment was set at 100%. Shown below are the EC_{50} values. (C) Experimental flow chart. Tet-On Aβ-GFP 293 cells were plated on day 1. On day 2, the cells were treated with curcumin, VB-030, or VB-037 for 8 h; addition of doxycycline (Dox, 2 μg/mL) followed. GFP fluorescence, Aβ-GFP messenger RNA (mRNA), and ROS were assessed on day 5. (D) Fluorescent images of Aβ-GFP cells untreated or treated with curcumin or VB-037 (5 μM). Nuclei were counterstained with Hoechst 33342 (blue). (E) GFP fluorescence assay with curcumin, VB-030, or VB-037 (1.2–10 μM) treatment ($n = 3$). The relative GFP fluorescence of untreated cells (Untr.) was normalized as 100%. GFP fluorescence was measured in wells containing at least 80% viable cells. Shown below are IC_{50} values determined by the percentage of survived cells. (F) Real-time PCR quantification of the Aβ-GFP mRNA level relative to HPRT1 mRNA in untreated cells and cells treated with curcumin, VB-030, or VB-037 (5 μM) ($n = 3$). (G) ROS assay with curcumin, VB-030, or VB-037 (5 μM) treatment ($n = 3$). The relative ROS of uninduced cells (without Dox) was normalized (100%).

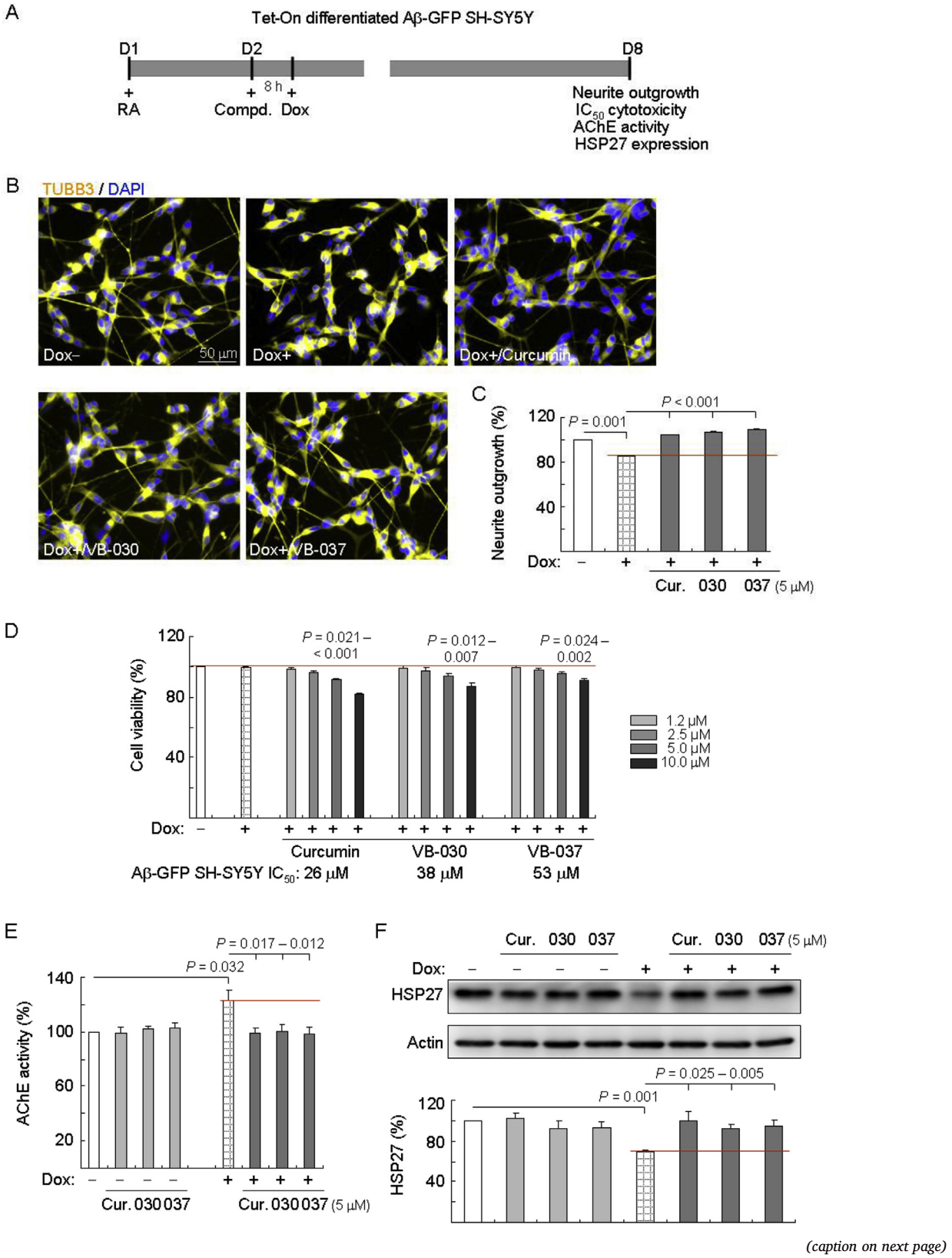

(caption on next page)

overexpression (from 126% to 107%–83%; $P = 0.003$–0.001) (Fig. 1G). These results suggested that VB-030 and VB-037 not only inhibited Aβ aggregation but also reduced ROS induced by Aβ overexpression.

3.2. Effects of tested compounds on Aβ-GFP-expressing SH-SY5Y cells

The neuroprotective effects of VB-030 and VB-037 were evaluated using Aβ-GFP-expressing SH-SY5Y cells (Fig. 2A and B). Aβ-GFP-expressing SH-SY5Y cells were generated through stable integration of a single-copy Aβ-GFP gene with 25–30 iterations of RNA expression in an

Fig. 2. Neuroprotective effects of test compounds on Tet-On Aβ-GFP SH-SY5Y cells. (A) Experimental flow chart. On day 1, the cells were plated with retinoic acid (RA; 10 μM). On day 2, curcumin, VB-030, or VB-037 was added to the cells for 8 h, followed by induction of Aβ-GFP overexpression with doxycycline (Dox, 2 μg/mL) for 6 days. On day 8, neurite outgrowth was measured. In addition, cell viability, AChE activity, and HSP27 expression were examined. (B) Fluorescence microscopy images of differentiated Aβ-GFP SH-SY5Y cells uninduced (Dox-), untreated (Dox+), or treated with curcumin, VB-030, or VB-037 (5 μM). TUBB3 staining was performed to quantify the extent of neurite outgrowth. Nuclei were counterstained with DAPI (blue). (C) Quantification of neurite outgrowth in cells treated with curcumin, VB-030, or VB-037 (5 μM) ($n = 3$). The relative neurite outgrowth of uninduced cells was normalized as 100%. *P* values: comparisons between induced (Dox+) and uninduced (Dox-) cells or between treated (Dox+/compound) and untreated (Dox+) cells. (D) Cytotoxicity of test compounds in Aβ-GFP SH-SY5Y cells examined using the PI assay. Cells were treated with curcumin, VB-030, or VB-037 (1.2–10 μM), and cell viability was measured on day 8 ($n = 3$). To normalize, the relative viability of uninduced cells was set at 100%. IC_{50} values are presented below. (E) AChE activity of cells treated with curcumin, VB-030, or VB-037 (5 μM) in SH-SY5Y cells without or with Aβ expression ($n = 3$). The relative AChE activity of uninduced and untreated cells was normalized to 100%. *P* values: comparisons between induced and uninduced cells or between treated and untreated cells. (F) HSP27 expression of cells with curcumin, VB-030, or VB-037 (5 μM) treatment in SH-SY5Y cells without or with Aβ expression ($n = 3$). The relative HSP27 level of uninduced and untreated cells was normalized to 100%. *P* values: comparisons between induced and uninduced cells or between treated and untreated cells.

inducible fashion (Chang et al., 2016). Under neuronal differentiation with retinoic acid (10 μM) for 1 week, more than 90% of the Aβ-GFP-expressing cells were viable, and Aβ overexpression significantly reduced the neurite length (from 100% to 86%; $P = 0.001$; Fig. 2C and D). Pretreatment with curcumin, VB-030, or VB-037 (5 μM) successfully rescued this impairment of neurite outgrowth (from 86% to 105%–109%; $P < 0.001$) (Fig. 2C). The IC_{50} values of curcumin, VB-030, and VB-037 in retinoic acid-differentiated Aβ-GFP-expressing SH-SY5Y cells were 26, 38, and 53 μM, respectively (Fig. 2D).

In the brains of AD patients, Aβ aggregates colocalize with AChE, which accelerates assembly of Aβ peptides into Alzheimer fibrils (Inestrosa et al., 1996). Our Aβ-GFP-expressing SH-SY5Y cells successfully recapitulated this key disease feature and exhibited increased AChE activity (123%, $P = 0.032$), as demonstrated by Aβ overexpression (Fig. 2E). Treatment with curcumin, VB-030, or VB-037 (5 μM) attenuated the AChE hyperactivity induced by Aβ overexpression (from 123% to 101%–98%; $P = 0.017$–0.012) (Fig. 2E), whereas these compounds did not exert any effects on the AChE activity of SH-SY5Y cells without Aβ expression (99%–103%, $P > 0.05$). The small molecular chaperone HSP27 is involved in inhibition of Aβ aggregation (Wilhelmus et al., 2006a). In Aβ-GFP-expressing SH-SY5Y cells, Aβ overexpression significantly downregulated HSP27 (69%, $P = 0.001$), whereas treatment with curcumin, VB-030, or VB-037 (5 μM) significantly upregulated HSP27 expression (from 69% to 92%–100%; $P = 0.025$–0.005) (Fig. 2F). Nevertheless, enhancement of HSP27 level by curcumin, VB-030, or VB-037 was not observed in SH-SY5Y cells without Aβ expression (92%–103%, $P > 0.05$). These results suggested that VB-030 and VB-037 exerted neuroprotective effects on Tet-On Aβ-GFP-expressing SH-SY5Y cells. In addition, VB-030 and VB-037 downregulated AChE activity and upregulated HSP27 expression in Tet-On Aβ-GFP-expressing SH-SY5Y cells.

3.3. HSP27 as a therapeutic target in VB-compound-treated Aβ-GFP-expressing SH-SY5Y cells

To validate the potential of HSP27 as a therapeutic target of VB compounds, we knocked down HSP27 expression through lentivirus-mediated shRNA targeting of HSP27 in Aβ-GFP-expressing SH-SY5Y cells (Fig. 3A). In scrambled shRNA-infected cells, Aβ overexpression significantly downregulated HSP27 expression (64%, $P = 0.037$). In addition, treatment with curcumin, VB-030, or VB-037 significantly increased HSP27 expression (93%–96%, $P = 0.035$–0.025). These upregulations were counteracted by HSP27-specific shRNA (60%–51%, $P = 0.045$–0.021) (Fig. 3B). In line with HSP27 expression, the increased level of soluble Aβ-GFP after treatment with curcumin, VB-030, or VB-037 (116%–131%, $P = 0.044$–0.021) was significantly reduced by HSP27-specific shRNA (91%–102%, $P = 0.019$–0.012) (Fig. 3B). Furthermore, improvement in neurite outgrowth by curcumin, VB-030, or VB-037 (scrambled: 107%–109%; $P = 0.002$ to < 0.001 compared with no treatment: 88%) was significantly attenuated by HSP27 shRNA knockdown (89%–97%, $P = 0.005$ to < 0.001) (Fig. 3C and D). These results suggested that VB-030 and VB-037 exerted neuroprotective effects by upregulating HSP27 expression.

3.4. Effects of VB-037 on LPS/IFN-γ-activated BV-2 cells

In the brain, activated microglia release proinflammatory mediators in response to neuroinflammation (McGeer et al., 1993). Therefore, we investigated the antineuroinflammatory effects of VB compounds on BV-2 microglial cells. VB-037 had a higher IC_{50} values (65 μM) than did VB-030 (39 μM) in BV-2 cells (Fig. 4A); therefore, VB-037 was chosen for further assessment with LPS/IFN-γ-stimulated BV-2 microglia (Brown et al., 2014) (Fig. 4B). As shown in Fig. 4C, the resting BV-2 microglia exhibited a ramified morphology. After LPS (1 μg/mL) and IFN-γ (0.1 μg/mL) stimulation for 20 h, cells were activated and became elongated with extended processes. Treatment with VB-037 for 8 h mitigated this activated morphology. The production of NO in the cultured medium (454%, $P = 0.021$) and expression of the activated microglia marker Iba1 (237%, $P = 0.014$) were significantly increased after LPS/IFN-γ stimulation, whereas treatment with VB-037 (10 μM) significantly reduced NO production (from 454% to 192%; $P = 0.040$) and Iba1 expression (from 237% to 158%; $P = 0.032$) (Fig. 4D and E). These results suggested that VB-037 was able to reduce the microglial activation states.

3.5. Effects of VB-037 on LPS/IFN-γ stimulated Aβ-GFP-expressing SH-SY5Y cells

LPS—a TLR4 agonist (Beutler, 2009)—leads to induction of proinflammatory genes in SH-SY5Y cells (Lawrimore and Crews, 2017), whereas treatment of neuronal cells with IFN-γ increases neuronal death in response to Aβ (Bate et al., 2006). Neuroinflammation is also linked to caspase-1-mediated IL-1β activation (Kaushal et al., 2015). Thus, we applied LPS (1 μg/mL) and IFN-γ (0.1 μg/mL) to the retinoic-acid-differentiated Aβ-GFP-expressing SH-SY5Y cells for 2 days to model neuroinflammatory damage to neurons in AD patients (Fig. 5A). As shown in Fig. 5B, addition of LPS/IFN-γ in differentiated Aβ-GFP-expressing SH-SY5Y cells resulted in a significant decrease in cell viability (80%, $P = 0.014$). Treatment with VB-037 or curcumin significantly improved cell viability (94%–95%, $P = 0.011$–0.010) (Fig. 5B). Furthermore, the upregulation of caspase 1 activity (161%, $P < 0.001$) and IL-1β (150%, $P < 0.001$), TNF-α (162%, $P = 0.007$), and IL-6 (268%, $P = 0.016$) expression in differentiated Aβ-GFP-expressing SH-SY5Y cells caused by 2 days of LPS/IFN-γ stimulation was mitigated by treatment with VB-037 or curcumin (caspase activity: 128%–134%, $P < 0.001$; IL-1β: 116%–115%, $P < 0.001$; TNF-α: 111%–121%, $P = 0.006$–0.008; IL-6: 137%–157%, $P = 0.015$–0.017) (Fig. 5C and D). Neither VB-037 nor curcumin had any effect on IL-1β, TNF-α, or IL-6 expression in SH-SY5Y cells without Aβ-GFP induction or LPS/IFN-γ exposure (93%–103%, $P > 0.05$; Fig. 5D).

Upon binding to the IL-1 receptor and accessory proteins, IL-1β triggers activation of signaling pathways, including P38 and JNK mitogen-activated protein kinase pathways (O'Neill, 2002), both of which play a critical role in inflammatory cell signaling (Goldstein and

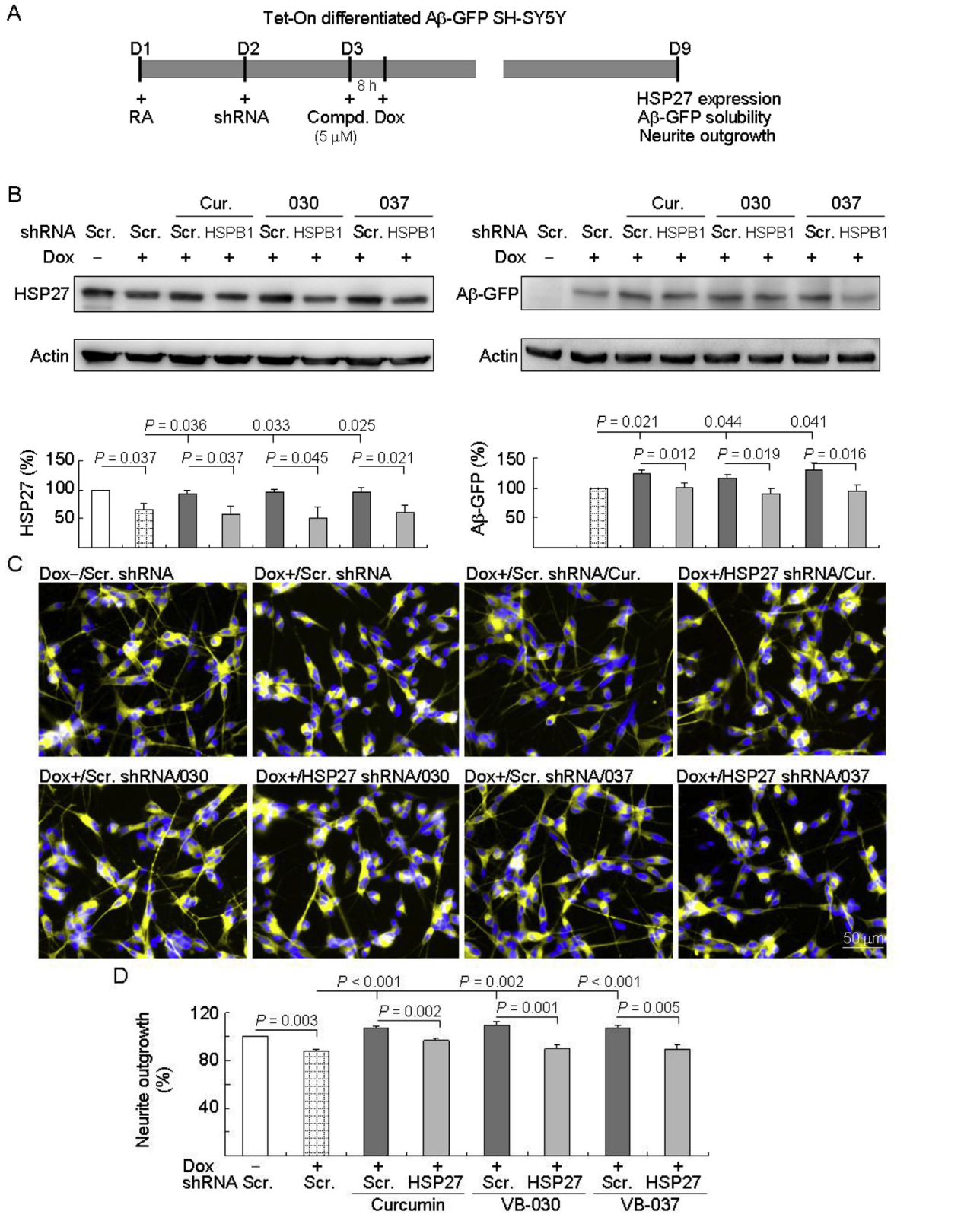

(caption on next page)

Gabriel, 2005; Cui et al., 2007). As shown in Fig. 5E, phosphor/total ratios of P38 (124%, $P = 0.036$), JNK (114%, $P = 0.018$), and JUN (126%, $P = 0.029$) were significantly increased after addition of LPS/IFN-γ to differentiated Aβ-GFP-expressing SH-SY5Y cells, whereas treatment with VB-037 or curcumin reduced the phosphor/total ratios of P38 (from 124% to 86%–84%; $P = 0.004$–0.005), JNK (from 114% to 98%–92%; $P = 0.004$–0.001), and JUN (from 126% to 84%–79%; $P = 0.011$–0.002). These results demonstrated the antineuroinflammatory effect of VB-037 on AD neuronal models.

Fig. 3. HSP27 as a therapeutic target in VB-compound-treated Aβ-GFP SH-SY5Y cells. (A) Experimental flow chart. On day 1, Aβ-GFP SH-SY5Y cells were plated with retinoic acid (RA; 10 μM). On day 2, the cells were infected with lentivirus-expressing HSP27-specific or scrambled shRNA. At 24 h postinfection, curcumin, VB-030, or VB-037 (5 μM) was added to the cells for 8 h, followed by induction of Aβ-GFP expression (Dox, 2 μg/mL) for 6 days. On day 9, the cells were collected for HSP27 and Aβ-GFP protein analyses through immunoblotting (β-actin as a loading control) and high-content neurite outgrowth analysis. (B) Western blot analysis of HSP27 and Aβ-GFP protein levels in compound-treated cells infected with HSP27-specific or scrambled shRNA-expressing lentivirus. To normalize, the relative HSP27 level of uninduced cells or the Aβ-GFP level of untreated cells was set at 100%. *P* values: comparisons between induced and uninduced cells, between compound-treated and untreated cells, or between scrambled and HSP27 shRNA-infected cells ($n = 3$). (C) Microscopic images of uninduced or induced Aβ-GFP SH-SY5Y cells with scrambled or HSP27-specific shRNA or compound (5 μM) treatments. TUBB3 staining was used to quantify the extent of neurite outgrowth. Nuclei were counterstained with DAPI (blue). (D) Neurite outgrowth assay of compound-treated Aβ-GFP SH-SY5Y cells infected with HSP27-specific or a scrambled shRNA. To normalize, the relative neurite outgrowth of uninduced cells infected with scrambled shRNA without compound treatment was set at 100%. *P* values: comparisons between induced and un-induced cells, between compound-treated and untreated cells, or between scrambled shRNA and HSP27-specific shRNA-infected cells ($n = 3$).

4. Discussion

Lines of evidence have shown the crucial role of misfolded Aβ in the pathogenesis of AD (Selkoe and Hardy, 2016), and strategies to reduce Aβ production or enhance Aβ clearance have been suggested as therapeutic strategies for AD (Barage and Sonawane, 2015). In addition, chemical or molecular chaperones are another possible target class for therapeutic intervention in protein misfolding disease states. For example, several heterocyclic aromatic organic compounds including indoles and quinolines have been identified as chemical chaperones that can help refold Aβ with conformational changes (Chang et al., 2016). In the present study, in addition to the chemical chaperone activity in the thioflavin T assay, we demonstrated that the quinoline compounds VB-030 and VB-037 could reduce Aβ misfolding and promote neurite outgrowth by upregulating the small molecular chaperone HSP27 in Aβ-GFP-expressing 293/SH-SY5Y AD cell models (Figs. 1 and 2). VB-037 further attenuated LPS/IFN-γ-induced microglial activation and neuroinflammation signaling pathways in the Aβ-GFP-expressing SH-SY5Y neuroblastoma cell model (Figs. 4 and 5). These findings supported the potential of VB-037 as a novel Aβ aggregation inhibitor with antineuroinflammatory activity for AD treatment.

Amyloid plaques are a central feature of AD pathology and are considered a major factor in neuronal cell loss (Hardy and Higgins, 1992). Ultrastructurally, plaques are fibrous masses composed primarily of Aβ (Jarrett et al., 1993), which is derived through endoproteolysis of the integral membrane APP that results in secretion of

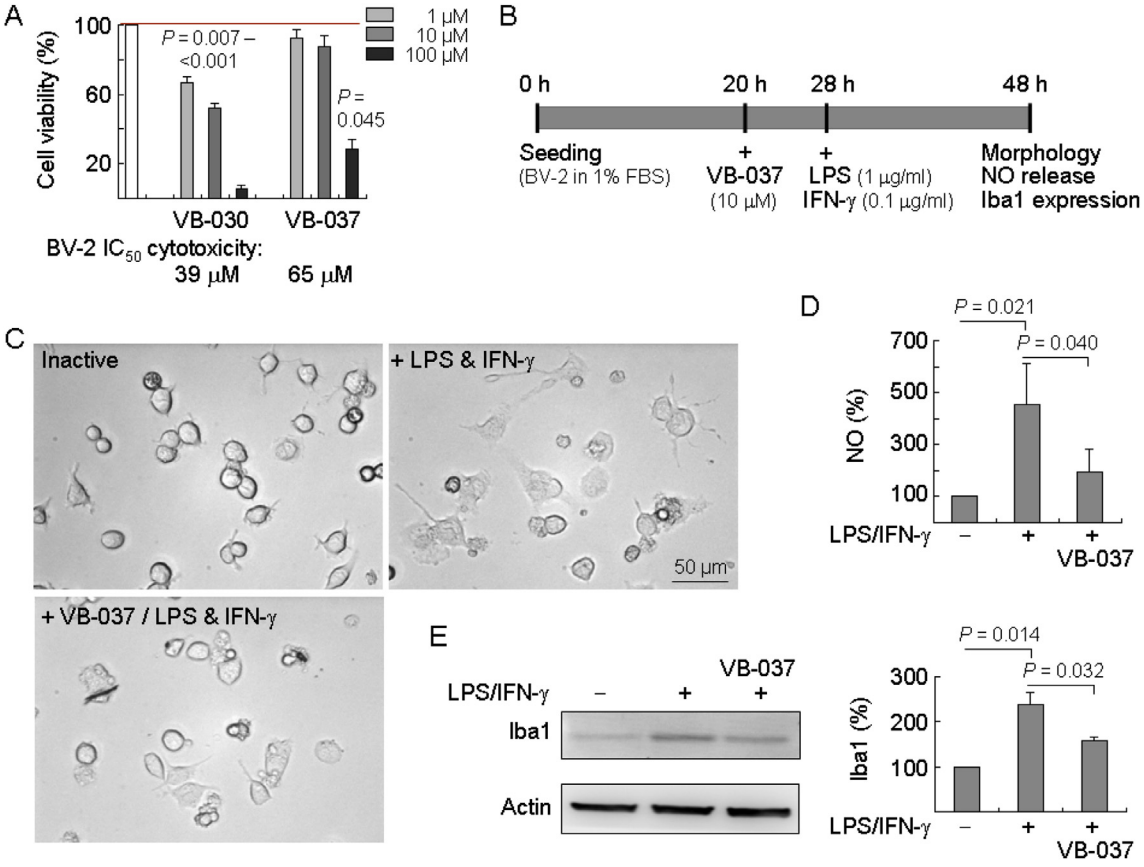

Fig. 4. Anti-inflammatory activity of VB-037 in LPS and IFN-γ-activated BV-2 cells. (A) Cytotoxicity of VB compounds against BV-2 examined using the MTT assay. Cells were treated with VB-030 or VB-037 (1–100 μM) and cell viability was measured the next day ($n = 3$). To normalize, the relative viability of untreated cells was set at 100%. IC_{50} values are presented below. (B) Experimental flow chart. BV-2 cells were plated in 1% FBS at 0 h. After 20 h, the cells were pretreated with VB-037 (10 μM) for 8 h, followed by LPS (1 μg/mL) and IFN-γ (0.1 μg/mL) treatment to induce activation. After 20 h, the cells were examined for microglial activation by morphology, NO release in cell culture medium, and Iba1 Western blotting. (C) Morphology of inactive BV-2 cells, activated by LPS and IFN-γ or pretreated with VB-037 (+VB-037/LPS & IFN-γ). (D) NO production of LPS/IFN-γ-activated BV-2 cells pretreated with VB-037 ($n = 3$). For normalization, the relative NO level in the cell culture medium prepared from inactive cells was set as 100%. *P* values: comparisons between inactive and activated cells or between treated and untreated cells. (E) Iba1 level of LPS/IFN-γ-activated BV-2 pretreated with VB-037 ($n = 3$). For normalization, the relative Iba1 level in the cell lysate prepared from inactive cells was set as 100%. *P* values: comparisons between inactive and activated cells, or between treated and untreated cells.

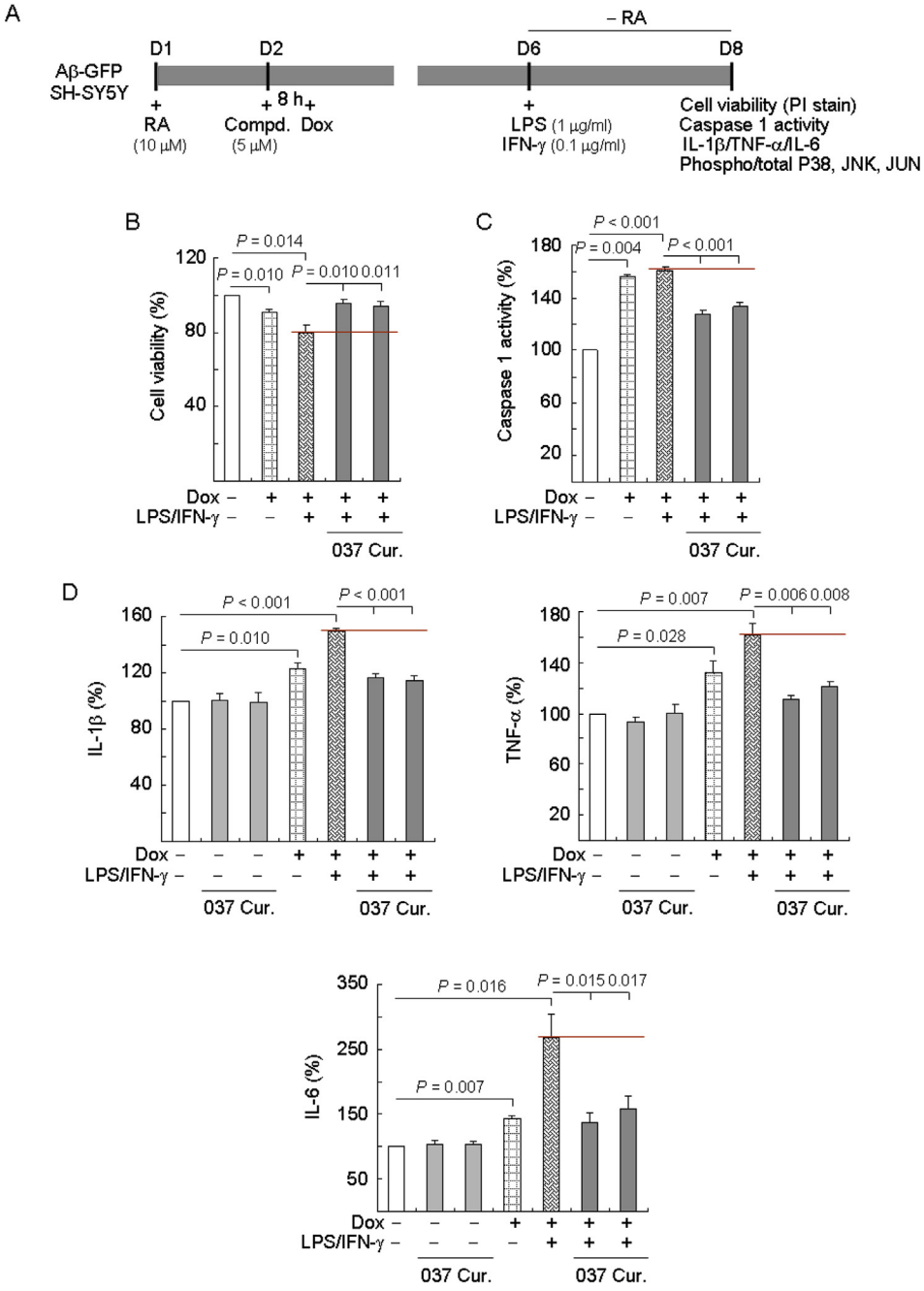

Fig. 5. Neuroprotection of VB-037 in LPS and IFN-γ-stimulated Aβ-GFP SH-SY5Y cells. (A) Experimental flow chart. On day 1, Aβ-GFP SH-SY5Y cells were plated with retinoic acid (RA; 10 μM). On day 2, compound (5 μM) was added to the cells for 8 h; induction of Aβ-GFP overexpression (Dox, 2 μg/mL) followed. On day 6, retinoic acid was removed and LPS (1 μg/mL) and IFN-γ (0.1 μg/mL) were added to the cells. Cell viability (by PI staining); caspase 1 activity (by the fluorimetric assay); IL-1β, TNF-α, and IL-6 levels; and phospho/total P38, JNK, and JUN ratios (by immunoblotting) were examined on day 8. Cell viability (B); caspase 1 activity (C); IL-1β, TNF-α, and IL-6 levels (D); and phospho/total P38, JNK, and JUN ratios (E) of LPS/IFN-γ-stimulated Aβ-GFP SH-SY5Y pretreated with VB-037 or curcumin. To normalize, the relative level of cells without Dox induction and LPS/IFN-γ stimulation was set at 100%. *P* values: comparisons between induced and stimulated versus uninduced and unstimulated cells or between compound-treated and untreated cells ($n = 3$).

the peptide by normal cellular pathways, as well as intracellular accumulation. Under pathogenic conditions, Aβ self-associates into a well-defined supramolecular fibril with a high β-sheet content (Inouye et al., 1993). Aβ aggregation is a multistage process initiated by association of individual Aβ monomers into small nucleating "seeds" and accompanied by a transition from a predominately random coil to an amyloidogenic β-sheet conformation (Lomakin et al., 1997). Aβ seeds subsequently assemble in an intermediate protofibrillar structure, which further converts to ramified fibrils (Walsh et al., 1997). Formation of Aβ fibrils can be affected by chaperones that may control Aβ self-association. Chaperones can be classified into chemical and molecular groups. Chemical chaperones are low-molecular-weight compounds that specifically bind to proteins and induce refolding or structural stabilization. In the thioflavin T assay, VB-030 and VB-037 demonstrated their potential as chemical chaperones for reduction of Aβ misfolding (Fig. 1). Interaction between these quinoline compounds and Aβ likely leads to strong hydrophobic interactions, which may disrupt fibrils formation and prevent oligomerization (Kundaikar and Degani, 2015). A comprehensive structural activity analysis could be helpful to reveal atomistic mechanisms underlying inhibition of Aβ

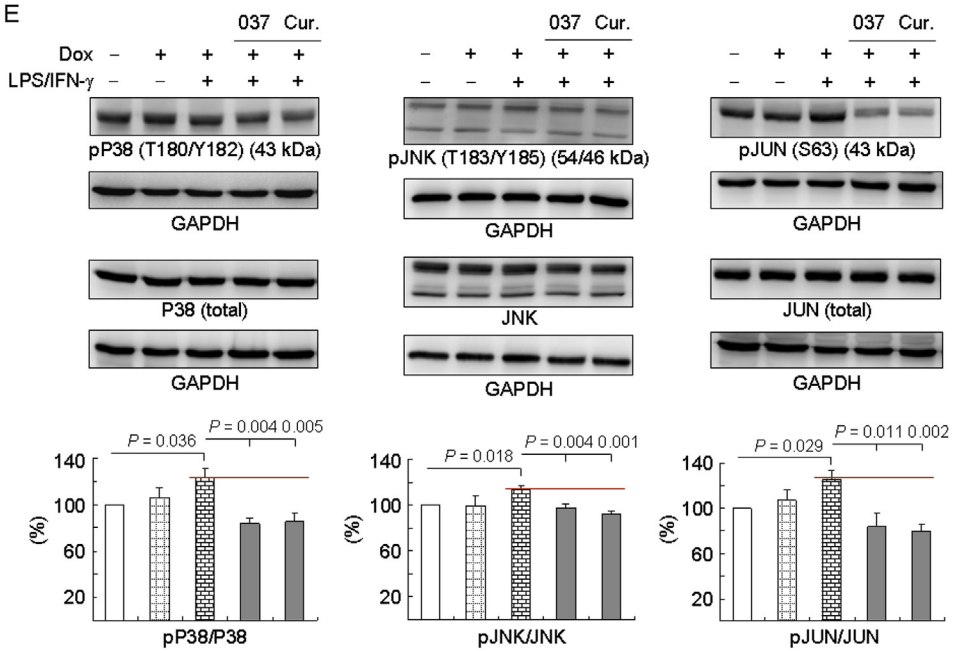

Fig. 5. (*continued*)

aggregation by quinoline derivatives.

In this study, VB-030 and VB-037 modulated Aβ aggregation by upregulating the molecular chaperone HSP27 and downregulating AChE activity (Fig. 2). HSP27 is a small molecular chaperone that reduces Aβ aggregation (Wilhelmus et al., 2006a). Extracellular expression of HSP27 was observed in the senile plaques of AD brains; in addition, HSP27 was observed in astrocytes associated with senile plaques (Wilhelmus et al., 2006b). Overexpression of HSP27 inhibited Aβ-mediated toxicity in cultured cortical neurons (King et al., 2009) and reduced deposition of Aβ plaques in APP/PS1 mice (Tóth et al., 2013). Moreover, HSP27 directly mediates neurite outgrowth beyond the chaperoning of misfolded proteins. In the neurons of the dorsal root ganglion, overexpression of HSP27 positively affects neurite outgrowth, whereas HSP27 knockdown reduces neurite complexity and length (Williams et al., 2006). Inhibition of HSP27 phosphorylation generates an atypical growth pattern in the neurons of the dorsal root ganglion (Williams et al., 2005); this pattern is linked to the ability of HSP27 to regulate cytoskeletal stability. Furthermore, HSP27 silencing also suppressed both pituitary adenylate cyclase-activating polypeptide 38- and Rin-mediated neurite outgrowth in PC6 cells, thereby supporting the role of HSP27 in neurite outgrowth (Shi et al., 2008). Our study results showed that VB-030 and VB-037 prevented Aβ-mediated neurite outgrowth impairment by upregulating HSP27 (Figs. 2 and 3), thereby consolidating the role of these small molecules in improving neurite outgrowth.

Evidence suggests that Aβ affects expression of AChE. Aβ increased AChE activity in the primary cultures of cortical neurons and astrocytes (Sáez-Valero et al., 2003). AChE level was also increased in the cortex of rat that received intracerebroventricular injections of Aβ (Sáez-Valero et al., 2002). In AD patients, AChE level increased around amyloid plaques and in tangle-bearing neurons (Morán et al., 1994). AChE may play a role in Aβ fibrillogenesis by promoting and accelerating the generation of Aβ fibrils (Inestrosa et al., 1996). Amyloid plaques appeared sooner and were more prominent in APP and AChE double-transgenic mice than in parental APP transgenic mice (Rees et al., 2003). Although the disease-modifying benefits of AChE inhibitors for AD remain controversial, the inhibition of AChE activity by VB-030 and VB-037 (Fig. 2) indicates that these compounds may modulate Aβ misfolding by downregulating AChE.

Aβ accumulation promotes significant neuroinflammation by activating microglia. Overproduction of pro-inflammatory cytokines (IL-1β, TNF-α, IFN-γ, and IL-6) by activated microglia upregulates the activities of β- and γ-secretases, thereby promoting Aβ production (Hickman et al., 2008). By contrast, emerging evidence indicates that infectious agents such as bacterial LPS may be crucial for triggering Aβ-mediated neurotoxicity. LPS colocalizes with Aβ in the amyloid plaques of AD patients (Zhan et al., 2016). LPS and Aβ bind to the TLR4 receptor (Tang et al., 2008; Beutler, 2009; Vollmar et al., 2010) and upregulate caspase 1 and IL-1β in human neurons (Kaushal et al., 2015). IL-1β activates inflammatory signaling such as the JNK and P38 pathways (O'Neill, 2002), both of which are involved in AD pathology and neurodegeneration (Atzori et al., 2001; Savage et al., 2002). Furthermore, upregulation of IL-1β promotes Aβ accumulation (Griffin et al., 1998), thereby initiating a vicious feedback loop for Aβ cascade. In the present study, VB-037 demonstrated inhibitory potential for microglial activation and Aβ/LPS-induced neuroinflammation in Aβ-GFP-expressing SH-SY5Y cells (Figs. 4 and 5), indicating that VB-037 plays a role in AD treatment by blocking this vicious cycle of neuroinflammation. The anti-inflammatory property of VB-037 may be a result of its quinoline structure, which can occupy the COX-2 active site and demonstrate strong inhibitory potential for COX-2 (Hosseinzadeh et al., 2017).

In our study, VB-037 reduced Aβ-induced oxidative stress in the Aβ-GFP-expressing 293 model (Fig. 1). VB-037 possesses a structure of tetrahydro-1,4-oxazine (C_4H_9NO). Derivatives of tetrahydro-1,4-oxazine demonstrated potential against lipid peroxidation (Kourounakis et al., 2008). The antioxidative effect of the 1,4-oxazine structure may also contribute to neuroprotection of VB-037 in an AD model.

Lipinski's rule of 5, including a molecular weight (MW) of ≤500 Da, ≤5 hydrogen bond donors (HBDs), ≤10 hydrogen bond acceptors (HBAs), and a CLog P of ≤5 (the octanol-water partition coefficient measures the lipophilicity of a compound), is commonly used to predict the bioavailability of oral medications (Lipinski et al., 1997). With an MW of 296.4–412.4 Da, 0 HBDs, 2–7 HBAs, and a Clog P of 5.0–4.5, both VB-030 and VB-037 meet Lipinski's criteria (ChemDraw; http://www.perkinelmer.com/tw/category/chemdraw) and are believed to demonstrate high oral bioavailability. Simple diffusion through the blood-brain barrier (BBB) is another important aspect of drug development targeting neurodegenerative diseases. According to the online BBB predictor (https://www.cbligand.org/BBB/) (Zhao et al., 2007),

both VB-030 and VB-037 can diffuse across the BBB. Additional *in vivo* experimental approaches are required to clarify these concerns regarding VB-030 and VB-037.

The multifactorial nature of AD requires simultaneous modulation of multiple targets to manage disease progression, leading to an urgent need for multitarget drugs. For example, curcumin may modify AD pathology by inhibiting Aβ formation and aggregation, AChE activity, and microglial activation, as well as by mediating the insulin signaling pathway (Tang and Taghibiglou, 2017). In this study, VB-037 demonstrated Aβ aggregation inhibition and neuroprotection through upregulation of chaperones, reduction of AChE activity, microglial activation, and neuroinflammation, thereby indicating its potential as a novel compound with multiple targets for treating AD. Compared with curcumin, VB-037 demonstrated lower cellular toxicity (Figs. 1 and 2), suggesting a wide therapeutic window for treatment. Future *in vivo* and clinical studies are warranted to provide a promising avenue for application of VB-037 to modify the disease progression of AD patients.

5. Conclusions

In summary, our findings indicated that Aβ misfolding increased AChE activity and ROS levels, as well as neuronal damage. The novel compound VB-037 could reverse these negative effects of Aβ overexpression, reduce neuroinflammation, and directly inhibit Aβ aggregation. VB-037 improved neuronal damage and neuroinflammation by regulating the chaperone HSP27 and the P38/JNK signaling pathway. These findings strongly support the potential of VB-037 as a novel multitarget therapeutic candidate for treating AD.

Conflicts of interest

The authors declare that there is no conflict of interest.

Acknowledgment

We thank the Molecular Imaging Core Facility of National Taiwan Normal University for the technical assistance. This work was supported by the grants 105-2325-B-003-001, 106-2314-B-182-037-MY2, and 107-2320-B-003-006 from the Ministry of Science and Technology, and CMRPG3F1611-13 from Chang Gung Medical Foundation, Taiwan.

References

Abdallah, M., Jacqueline, C., Anne, D.R., Jacques, B., Jean-Marie, P., 2006. Quinoline derivatives as promising inhibitors of antibiotic efflux pump in multidrug resistant *Enterobacter aerogenes* isolates. Curr. Drug Targets 7, 843–847.

Atzori, C., Ghetti, B., Piva, R., Srinivasan, A.N., Zolo, P., Delisle, M.B., Mirra, S.S., Migheli, A., 2001. Activation of the JNK/p38 pathway occurs in diseases characterized by tau protein pathology and is related to tau phosphorylation but not to apoptosis. J. Neuropathol. Exp. Neurol. 60, 1190–1197.

Balducci, C., Frasca, A., Zotti, M., La Vitola, P., Mhillaj, E., Grigoli, E., Iacobellis, M., Grandi, F., Messa, M., Colombo, L., Molteni, M., Trabace, L., Rossetti, C., Salmona, M., Forloni, G., 2017. Toll-like receptor 4-dependent glial cell activation mediates the impairment in memory establishment induced by β-amyloid oligomers in an acute mouse model of Alzheimer's disease. Brain Behav. Immun. 60, 188–197.

Barage, S.H., Sonawane, K.D., 2015. Amyloid cascade hypothesis: pathogenesis and therapeutic strategies in Alzheimer's disease. Neuropeptides 52, 1–18.

Bate, C., Kempster, S., Last, V., Williams, A., 2006. Interferon-γ increases neuronal death in response to amyloid-β_{1-42}. J. Neuroinflammation 3, 7.

Beutler, B.A., 2009. TLRs and innate immunity. Blood 113, 1399–1407.

Blasi, E., Barluzzi, R., Bocchini, V., Mazzolla, R., Bistoni, F., 1990. Immortalization of murine microglial cells by a v-raf/v-myc carrying retrovirus. J. Neuroimmunol. 27, 229–237.

Brown, D., Tamas, A., Reglodi, D., Tizabi, Y., 2014. PACAP protects against inflammatory-mediated toxicity in dopaminergic SH-SY5Y cells: implication for Parkinson's disease. Neurotox. Res. 26, 230–239.

Calvo-Rodríguez, M., de la Fuente, C., García-Durillo, M., García-Rodríguez, C., Villalobos, C., Núñez, L., 2017. Aging and amyloid β oligomers enhance TLR4 expression, LPS-induced Ca^{2+} responses, and neuron cell death in cultured rat hippocampal neurons. J. Neuroinflammation 14, 24.

Chang, K.H., Chiu, Y.J., Chen, S.L., Huang, C.H., Lin, C.H., Lin, T.H., Lee, C.M., Ramesh, C., Wu, C.H., Huang, C.C., Fung, H.C., Chen, Y.C., Lin, J.Y., Yao, C.F., Huang, H.J., Lee-Chen, G.J., Lee, M.C., Hsieh-Li, H.M., 2016. The potential of synthetic indolylquinoline derivatives for Aβ aggregation reduction by chemical chaperone activity. Neuropharmacology 101, 309–319.

Chang, K.H., Lin, C.H., Chen, H.C., Huang, H.Y., Chen, S.L., Lin, T.H., Ramesh, C., Huang, C.C., Fung, H.C., Wu, Y.R., Huang, H.J., Lee-Chen, G.J., Hsieh-Li, H.M., Yao, C.F., 2017. The potential of indole/indolylquinoline compounds in tau misfolding reduction by enhancement of HSPB1. CNS Neurosci. Ther. 23, 45–56.

Cui, J., Zhang, M., Zhang, Y.Q., Xu, Z.H., 2007. JNK pathway: diseases and therapeutic potential. Acta Pharmacol. Sin. 28, 601–608.

Czarnecka, K., Girek, M., Maciejewska, K., Skibiński, R., Jończyk, J., Bajda, M., Kabziński, J., Sołowiej, P., Majsterek, I., Szymański, P., 2017. New cyclopentaquinoline hybrids with multifunctional capacities for the treatment of Alzheimer's disease. J. Enzym. Inhib. Med. Chem. 33, 158–170.

da Cruz e Silva, E.F., da Cruz e Silva, O.A., 2003. Protein phosphorylation and APP metabolism. Neurochem. Res. 28, 1553–1561.

Dal Prà, I., Chiarini, A., Gui, L., Chakravarthy, B., Pacchiana, R., Gardenal, E., Whitfield, J.F., Armato, U., 2015. Do astrocytes collaborate with neurons in spreading the "infectious" Aβ and Tau drivers of Alzheimer's disease? Neuroscientist 21, 9–29.

Desai, N.C., Joshi, V.V., Rajpara, K.M., Vaghani, H.V., Satodiya, H.M., 2013. Synthesis of quinoline-pyrazoline based thiazole derivatives endowed with antimicrobial activity. Indian J. Chem. 52B, 1191–1201.

Eswaran, S., Adhikari, A.V., Chowdhury, I.H., Pal, N.K., Thomas, K.D., 2010. New quinoline derivatives: synthesis and investigation of antibacterial and antituberculosis properties. Eur. J. Med. Chem. 45, 3374–3383.

Goldstein, D.M., Gabriel, T., 2005. Pathway to the clinic: inhibition of P38 MAP kinase. A review of ten chemotypes selected for development. Curr. Top. Med. Chem. 5, 1017–1029.

Griffin, W.S., Sheng, J.G., Royston, M.C., Gentleman, S.M., McKenzie, J.E., Graham, D.I., Roberts, G.W., Mrak, R.E., 1998. Glial-neuronal interactions in Alzheimer's disease: the potential role of a 'cytokine cycle' in disease progression. Brain Pathol. 8, 65–72.

Hardy, J.A., Higgins, G.A., 1992. Alzheimer's disease: the amyloid cascade hypothesis. Science 256, 184–185.

Hardy, J., 1997. Amyloid, the presenilins and Alzheimer's disease. Trends Neurosci. 20, 154–159.

Hickman, S.E., Allison, E.K., Khoury, J.E., 2008. Microglial dysfunction and defective β-amyloid clearance pathways in aging Alzheimer's disease mice. J. Neurosci. 28, 8354–8360.

Hosseinzadeh, H., Mazaheri, F., Ghodsi, R., 2017. Pharmacological effects of a synthetic quinoline, a hybrid of tomoxiprole and naproxen, against acute pain and inflammation in mice: a behavioral and docking study. Iran. J. Basic Med. Sci. 20, 446–450.

Inestrosa, N.C., Alvarez, A., Perez, C.A., Moreno, R.D., Vicente, M., Linker, C., Casanueva, O.I., Soto, C., Garrido, J., 1996. Acetylcholinesterase accelerates assembly of amyloid-β-peptides into Alzheimer's fibrils: possible role of the peripheral site of the enzyme. Neuron 16, 881–891.

Inouye, H., Fraser, P.E., Kirschner, D.A., 1993. Structure of β-crystallite assemblies formed by Alzheimer β-amyloid protein analogues: analysis by x-ray diffraction. Biophys. J. 64, 502–519.

Jarrett, J.T., Berger, E.P., Lansbury Jr., P.T., 1993. The carboxy terminus of the β amyloid protein is critical for the seeding of amyloid formation: implications for the pathogenesis of Alzheimer's disease. Biochemistry 32, 4693–4697.

Jones, M.R., Dyrager, C., Hoarau, M., Korshavn, K.J., Lim, M.H., Ramamoorthy, A., Storr, T., 2016. Multifunctional quinoline-triazole derivatives as potential modulators of amyloid-β peptide aggregation. J. Inorg. Biochem. 158, 131–138.

Kaushal, V., Dye, R., Pakavathkumar, P., Foveau, B., Flores, J., Hyman, B., Ghetti, B., Koller, B.H., LeBlanc, A.C., 2015. Neuronal NLRP1 inflammasome activation of Caspase-1 coordinately regulates inflammatory interleukin-1-beta production and axonal degeneration-associated Caspase-6 activation. Cell Death Differ. 22, 1676–1686.

King, M., Nafar, F., Clarke, J., Mearow, K., 2009. The small heat shock protein Hsp27 protects cortical neurons against the toxic effects of β-amyloid peptide. J. Neurosci. Res. 87, 3161–3175.

Kourounakis, A.P., Charitos, C., Rekka, E.A., Kourounakis, P.N., 2008. Lipid-lowering (hetero)aromatic tetrahydro-1,4-oxazine derivatives with antioxidant and squalene synthase inhibitory activity. J. Med. Chem. 51, 5861–5865.

Kundaikar, H.S., Degani, M.S., 2015. Insights into the interaction mechanism of ligands with Aβ42 based on molecular dynamics simulations and mechanics: implications of role of common binding site in drug design for Alzheimer's disease. Chem. Biol. Drug Des. 86, 805–812.

Lawrimore, C.J., Crews, F.T., 2017. Ethanol, TLR3, and TLR4 agonists have unique innate immune responses in neuron-like SH-SY5Y and microglia-like BV2. Alcohol Clin. Exp. Res. 41, 939–954.

LeVine 3rd, H., 1999. Quantification of β-sheet amyloid fibril structures with thioflavin T. Methods Enzymol. 309, 274–284.

Lieu, V.H., Wu, J.W., Wang, S.S., Wu, C.H., 2007. Inhibition of amyloid fibrillization of hen egg-white lysozymes by rifampicin and *p*-benzoquinone. Biotechnol. Prog. 23, 698–706.

Lipinski, C.A., Lombardo, F., Dominy, B.W., Feeney, P.J., 1997. Experimental and computational approaches to estimate solubility and permeability in drug discovery and development settings. Adv. Drug Deliv. Rev. 23, 3–25.

Lomakin, A., Teplow, D.B., Kirschner, D.A., Benedek, G.B., 1997. Kinetic theory of fibrillogenesis of amyloid β-protein. Proc. Natl. Acad. Sci. U.S.A. 94, 7942–7947.

McGeer, P.L., Kawamata, T., Walker, D.G., Akiyama, H., Tooyama, I., McGeer, E.G., 1993. Microglia in degenerative neurological disease. Glia 7, 84–92.

Morán, M.A., Mufson, E.J., Gómez-Ramos, P., 1994. Cholinesterases colocalize with sites of neurofibrillary degeneration in aged and Alzheimer's brains. Acta Neuropathol. 87, 284–292.

Mukherjee, S., Pal, M., 2013. Medicinal chemistry of quinolines as emerging anti-inflammatory agents: an overview. Curr. Med. Chem. 20, 4386–4410.
Navarrete, L.P., Guzmán, L., San Martín, A., Astudillo-Saavedra, L., Maccioni, R.B., 2012. Molecules of the quinoline family block tau self-aggregation: implications toward a therapeutic approach for Alzheimer's disease. J. Alzheimers Dis. 29, 79–88.
O'Neill, L.A., 2002. Signal transduction pathways activated by the IL-1 receptor/toll-like receptor superfamily. Curr. Top. Microbiol. Immunol. 270, 47–61.
Olajide, O.A., Bhatia, H.S., de Oliveira, A.C., Wright, C.W., Fiebich, B.L., 2013. Inhibition of neuroinflammation in LPS-activated microglia by cryptolepine. Evid. Based Complement. Altern. Med. 2013, 459723.
Pahlman, S., Ruusala, A.I., Abrahamsson, L., Mattsson, M.E., Esscher, T., 1984. Retinoic acid-induced differentiation of cultured human neuroblastoma cells: a comparison with phorbolester-induced differentiation. Cell Differ. 14, 135–144.
Pickhardt, M., Gazova, Z., von Bergen, M., Khlistunova, I., Wang, Y., Hascher, A., Mandelkow, E.M., Biernat, J., Mandelkow, E., 2005. Anthraquinones inhibit tau aggregation and dissolve Alzheimer's paired helical filaments *in vitro* and in cells. J. Biol. Chem. 280, 3628–3635.
Pitta, E., Rogacki, M.K., Balabon, O., Huss, S., Cunningham, F., Lopez-Roman, E.M., Joossens, J., Augustyns, K., Ballell, L., Bates, R.H., Van der Veken, P., 2016. Searching for new leads for tuberculosis: design, synthesis, and biological evaluation of novel 2-quinolin-4-yloxyacetamides. J. Med. Chem. 59, 6709–6728.
Querfurth, H.W., LaFerla, F.M., 2010. Alzheimer's disease. N. Engl. J. Med. 362, 329–344.
Rees, T., Hammond, P.I., Soreq, H., Younkin, S., Brimijoin, S., 2003. Acetylcholinesterase promotes beta-amyloid plaques in cerebral cortex. Neurobiol. Aging 24, 777–787.
Sáez-Valero, J., de Ceballos, M.L., Small, D.H., de Felipe, C., 2002. Changes in molecular isoform distribution of acetylcholinesterase in rat cortex and cerebrospinal fluid after intracerebroventricular administration of amyloid β-peptide. Neurosci. Lett. 325, 199–202.
Sáez-Valero, J., Fodero, L.R., White, A.R., Barrow, C.J., Small, D.H., 2003. Acetylcholinesterase is increased in mouse neuronal and astrocyte cultures after treatment with β-amyloid peptides. Brain Res. 965, 283–286.
Savage, M.J., Lin, Y.G., Ciallella, J.R., Flood, D.G., Scott, R.W., 2002. Activation of c-Jun N-terminal kinase and p38 in an Alzheimer's sisease model is associated with amyloid deposition. J. Neurosci. 22, 3376–3385.
Scheltens, P., Blennow, K., Breteler, M.M., de Strooper, B., Frisoni, G.B., Salloway, S., Van der Flier, W.M., 2016. Alzheimer's disease. Lancet 388, 505–517.
Selkoe, D.J., Hardy, J., 2016. The amyloid hypothesis of Alzheimer's disease at 25 years. EMBO Mol. Med. 8, 595–608.
Shi, G.X., Jin, L., Andres, D.A., 2008. Pituitary adenylate cyclase-activating polypeptide 38-mediated Rin activation requires Src and contributes to the regulation of Hsp27 signaling during neuronal differentiation. Mol. Cell Biol. 28, 4940–4951.
Sondag, C.M., Dhawan, G., Combs, C.K., 2009. Beta amyloid oligomers and fibrils stimulate differential activation of primary microglia. J. Neuroinflammation 6, 1.
Takasugi, N., Tomita, T., Hayashi, I., Tsuruoka, M., Niimura, M., Takahashi, Y., Thinakaran, G., Iwatsubo, T., 2003. The role of presenilin cofactors in the γ-secretase complex. Nature 422, 438–441.
Tang, S.C., Lathia, J.D., Selvaraj, P.K., Jo, D.G., Mughal, M.R., Cheng, A., Siler, D.A., Markesbery, W.R., Arumugam, T.V., Mattson, M.P., 2008. Toll-like receptor-4 mediates neuronal apoptosis induced by amyloid β-peptide and the membrane lipid peroxidation product 4-hydroxynonenal. Exp. Neurol. 213, 114–121.
Tang, M., Taghibiglou, C., 2017. The mechanisms of action of curcumin in Alzheimer's disease. J. Alzheimers Dis. 58, 1003–1016.
Tóth, M.E., Szegedi, V., Varga, E., Juhász, G., Horváth, J., Borbély, E., Csibrány, B., Alföldi, R., Lénárt, N., Penke, B., Sántha, M., 2013. Overexpression of Hsp27 ameliorates symptoms of Alzheimer's disease in APP/PS1 mice. Cell Stress Chaperones 18, 759–771.
Vollmar, P., Kullmann, J.S., Thilo, B., Claussen, M.C., Rothhammer, V., Jacobi, H., Sellner, J., Nessler, S., Korn, T., Hemmer, B., 2010. Active immunization with amyloid-β 1-42 impairs memory performance through TLR2/4-dependent activation of the innate immune system. J. Immunol. 185, 6338–6347.
Walsh, D.M., Lomakin, A., Benedek, G.B., Condron, M.M., Teplow, D.B., 1997. Amyloid β-protein fibrillogenesis. Detection of a protofibrilliar intermediate. J. Biol. Chem. 272, 22364–22372.
Wang, W.Y., Tan, M.S., Yu, J.T., Tan, L., 2015a. Role of pro-inflammatory cytokines released from microglia in Alzheimer's disease. Ann. Transl. Med. 3, 136.
Wang, X.Q., Xia, C.L., Chen, S.B., Tan, J.H., Ou, T.M., Huang, S.L., Li, D., Gu, L.Q., Huang, Z.S., 2015b. Design, synthesis, and biological evaluation of 2-arylethenylquinoline derivatives as multifunctional agents for the treatment of Alzheimer's disease. Eur. J. Med. Chem. 89, 349–361.
Wilhelmus, M.M., Boelens, W.C., Otte-Höller, I., Kamps, B., de Waal, R.M., Verbeek, M.M., 2006a. Small heat shock proteins inhibit amyloid-β protein aggregation and cerebrovascular amyloid-β protein toxicity. Brain Res. 1089, 67–78.
Wilhelmus, M.M., Otte-Höller, I., Wesseling, P., De Waal, R.M., Boelens, W.C., Verbeek, M.M., 2006b. Specific association of small heat shock proteins with the pathological hallmarks of Alzheimer's disease brains. Neuropathol. Appl. Neurobiol. 32, 119–130.
Williams, K.L., Rahimtula, M., Mearow, K.M., 2005. Hsp27 and axonal growth in adult sensory neurons *in vitro*. BMC Neurosci. 6, 24.
Williams, K.L., Rahimtula, M., Mearow, K.M., 2006. Heat shock protein 27 is involved in neurite extension and branching of dorsal root ganglion neurons *in vitro*. J. Neurosci. Res. 84, 716–723.
Yang, F., Lim, G.P., Begum, A.N., Ubeda, O.J., Simmons, M.R., Ambegaokar, S.S., Chen, P.P., Kayed, R., Glabe, C.G., Frautschy, S.A., Cole, G.M., 2005. Curcumin inhibits formation of amyloid β oligomers and fibrils, binds plaques, and reduces amyloid *in vivo*. J. Biol. Chem. 280, 5892–5901.
Zhan, X., Stamova, B., Jin, L.W., DeCarli, C., Phinney, B., Sharp, F.R., 2016. Gram-negative bacterial molecules associate with Alzheimer disease pathology. Neurology 87, 2324–2332.
Zhao, Y.H., Abraham, M.H., Ibrahim, A., Fish, P.V., Cole, S., Lewis, M.L., de Groot, M.J., Reynolds, D.P., 2007. Predicting penetration across the blood-brain barrier from simple descriptors and fragmentation schemes. J. Chem. Inf. Model. 47, 170–175.
Zhao, T., Zeng, Y., Kermode, A.R., 2012. A plant cell-based system that predicts Aβ42 misfolding: potential as a drug discovery tool for Alzheimer's disease. Mol. Genet. Metabol. 107, 571–579.